RSC Advances

RSC Advances

www.rsc.org/advances

This is an *Accepted Manuscript*, which has been through the Royal Society of Chemistry peer review process and has been accepted for publication.

Accepted Manuscripts are published online shortly after acceptance, before technical editing, formatting and proof reading. Using this free service, authors can make their results available to the community, in citable form, before we publish the edited article. This *Accepted Manuscript* will be replaced by the edited, formatted and paginated article as soon as this is available.

You can find more information about *Accepted Manuscripts* in the **Information for Authors**.

ROYAL SOCIETY OF CHEMISTRY

www.rsc.org/advances

Journal Name

Dynamic Article Links ▶

ARTICLE TYPE

Au decorated Fe$_3$O$_4$@TiO$_2$ magnetic composites with visible light-assisted enhanced catalytic reduction of 4-nitrophenol

Ying Zhou, Yihua Zhu,* Xiaoling Yang, Jianfei Huang, Wei Chen, Xiaoming Lv, Cuiyan Li and Chunzhong Li*

The heterostructured Au nanoparticles decorated Fe$_3$O$_4$@TiO$_2$ composite magnetic microspheres (MSs) were synthesized by grafting Au nanoparticles onto 3-Aminopropyltrimethoxysilane (APTMS) modified Fe$_3$O$_4$@TiO$_2$ MSs. Significantly, by varying the reaction conditions, the as-synthesized ₁₀ Fe$_3$O$_4$@TiO$_2$@Au MSs showed high performance in the catalytic reduction of 4-nitrophenol (4-NP) to 4-aminophenol (4-AP) in the presence of NaBH$_4$ under visible light. In addition, the as-prepared Fe$_3$O$_4$@TiO$_2$@Au MSs can clean themselves by photocatalytic degradation of organic molecules, and can be reused for several cycles with convenient magnetic separability. This approach provided a platform based on the synergy of varying components under suitable conditions to optimize the catalytic ability.

₁₅ 1. Introduction

In heterogeneous catalysis, reactants are absorbed on the surface of catalytically active solid. Most of such heterogeneous catalysts are typically composed of small particles of catalytically active materials, which can significantly enhance the contact between ₂₀ catalysts and surroundings, thus ensure the effectiveness of catalysts.[1] Au is usually chemically inert, however, the electronic properties of nanoparticles differ from the corresponding bulk materials, nanosized Au can be effective in the catalysis.[2] Gold nanoparticles (Au NPs) have been found to feature in several ₂₅ chemical reactions including low-temperature CO oxidation,[3] reductive catalysis of chlorinated or nitrogenated hydrocarbons,[4-6] and organic synthesis.[7,8] However, owing to the high surface energy, Au NPs are easy to aggregate leading to remarkable reduction even deactivation in their original catalytic activity.[9] ₃₀ Hence, Au NPs are generally immobilized onto a variety of supports including polymer,[10] metal oxides,[11-13] graphene oxide,[14] etc. Moreover, the synergistic interactions between metal nanoparticles and metal oxide supports contribute to the catalytic activity.[15] The composite way to produce new material could ₃₅ realize the combination or cooperation of the characteristics of each component leading to enhanced properties. In most cases, the recycle of such catalysts is tedious and time-consuming by centrifugation/redispersion thus hinders the effective recovery and reuse.[12]

₄₀ Fe$_3$O$_4$ nanoparticles have been extensively applied in many fields due to the rapid and efficient magnetic response by the aid of an external magnetic field. Their insoluble and superparamagnetic natures enable the separation of catalysts from reaction mixture trouble-free and efficient.[12] Recently, Fe$_3$O$_4$ ₄₅ nanoparticles have drawn attention as robust, readily available, high-surface-area supports in catalytic transformations.[16,17] However, Fe$_3$O$_4$ nanoparticles as supports are vulnerable to the

air. Thus, it is a need to build core/shell-structured composite carriers to hold Fe$_3$O$_4$ nanoclusters as core and functionalized ₅₀ layer as shell. The shells need to be chemically stable, convenient for the immobilization of Au NPs and beneficial for the catalytic reactions. On the basis of such consideration, TiO$_2$ can be an appropriate material, which possess high specific surface areas beneficial for the absorption of molecules, large pore volumes, as ₅₅ well as stable and interconnected frameworks with active pore surfaces for easy modification and functionalization.[13]

As reported by Kuroda et al., Au NPs directly deposited on poly(methyl methacrylate) (PMMA) beads, which showed a higher catalytic activity than AuNPs.[10] Esumi et al.[18] investigated ₆₀ the catalytic activity of dendrimer-stabilized nanoparticles. These authors demonstrated that the catalytic reaction was the diffusion controlled. So the exposed Au NPs in the reaction mixture is essential to achieve excellent catalytic efficiency. Up to now, there have been many efforts towards assembling noble-metal ₆₅ nanoparticles onto various supports with different structures. For example, Zhang et al.[19] have reported the synthesis of Au nanostructures on graphene oxide and their catalytic activity, but the rate constant of catalysis is moderate. What's more, it remains a difficult task to separate the catalysts from reaction solution. ₇₀ Chang et al.[20] have reported the structure of Ag decorated polyaniline nanofibers with Ag NPs exposed outside, the easy oxidation of Ag NPs may cause a reduction of catalytic activity and be negative to reuse. Zheng et al.[21] have synthesized Fe$_3$O$_4$@SiO$_2$@Au and such structure exhibited high catalytic ₇₅ activity. Efforts have been made to synthesize Au NPs decorated composite catalysts, while the response of noble metal to visible light is less reported. The localized surface plasmon resonance (LSPR) of Au NPs can bring several benefits to the catalysis when the system is exposed to visible light: heating effect, ₈₀ strengthened dipore-dipore reaction with polar molecule, as well

RSC Advances Accepted Manuscript

as the response of TiO_2 to visible light which contribute to the synergistic effect of noble catalysis and photocatalysis.[22]

Nitrophenols are among the common pollutants in the industrial and agricultural wastewater.[16] The removal of them can be realized by processes such as adsorption,[23] photocatalytic degradation,[24] microwave-assisted catalytic oxidation,[25] electro-Fenton method,[26] electrochemical treatment,[27] and so on. On the other hand, 4-aminophenol (4-AP) is of great importance in the manufacture of analgesic and antipyretic drugs.[28] 4-AP is also widely used as photographic developer, corrosion inhibitor, anticorrosion-lubricant, and hair-dyeing agent.[29] The reduction of 4-nitrophenol (4-NP) over Au nanocatalysts in the presence of $NaBH_4$ offers an effective way to the production of 4-AP. Also, the reduction has no byproducts formed and is easily monitored via UV-vis spectroscopy, which is suitable for the investigation of catalytic activity.

Herein, we report the synthesis of stable, reproducible and recyclable $Fe_3O_4@TiO_2@Au$ composites. The as-prepared multifunctional microspheres (MSs) have Fe_3O_4 core inside, TiO_2 interlayer and Au shell outside with uniform size range and areal distribution. These catalysts with the multicomponent nanostructure, designated $Fe_3O_4@TiO_2@Au$, are fabricated by uniform coating Fe_3O_4 with TiO_2 through sol-gel process and then with the modification of $Fe_3O_4@TiO_2$ MSs by 3-Aminopropyltrimethoxysilane (APTMS), followed by coating with a layer of citrate-stabilized Au NPs. The Au decorated $Fe_3O_4@TiO_2$ magnetic composites with visible light-assisted enhanced catalytic reduction of 4-NP were investigated. The catalytic activities of these composites have been tested by using the reduction of 4-NP to 4-AP as model reaction and monitored by UV-vis spectroscopy. The unique nanostructure makes the composite MSs stable, recyclable and high-enhancement in catalysis.

2. Experimental

2.1. Reagents and Materials

$FeCl_3.6H_2O$, Chloroauric acid, trisodium citrate, citric acid, sodium acetate, tetrabutyl titanate (TBOT), ethanol, ethylene glycol, NH_4F, aqueous ammonia (28 wt%) were of analytical grade and purchased from Shanghai Chemical Corp. 3-Aminopropyltrimethoxysilane (APTMS) were purchased from Sigma-Aldrich Chemicals Co. All chemicals were used as received. Ultrapure water (18 $M\Omega cm^{-1}$) was used for all experiments.

2.2. Synthesis of Fe_3O_4 MSs

Fe_3O_4 MSs were synthesized by the solvent-thermal method reported by Liu et al.[30] In a typical synthesis, 3.25 g of $FeCl_3.6H_2O$, 1.3 g of trisodium citrate and 6.0 g of sodium acetate were added into 100 mL of ethylene glycol under magnetic stirring. The mixture was then transferred and sealed into a Teflon-lined stainless-steel autoclave (200 mL in capacity). Then the reaction was allowed to proceed at 200 °C for 10 h. The obtained black products were collected using an external magnetic field, rinsed with deionized water and ethanol for 3 times, respectively. Finally, the obtained Fe_3O_4 MSs were dried in vacuum for 12 h.

2.3. Synthesis of $Fe_3O_4@TiO_2$ MSs

The Fe_3O_4 MSs with a uniform porous TiO_2 shell outside were performed following the sol-gel process described by Zhao group.[31] Typically, 0.075 g of Fe_3O_4, 0.3 mL of aqueous ammonia (28 wt%) were dissolved in 90 mL of ethanol and stirred for 15 min at 600 rpm at 45 °C. Then under continuous mechanical stirring, 0.75 mL of TBOT previously dissolved in 10 mL of ethanol was added dropwise into the mixture. The reaction was allowed to proceed at 45 °C for 24 h. The resultant products were separated and collected using an external magnetic field, rinsed with ethanol and water and then dried in vacuum for 12 h. To improve crystallinity, 0.4 g of $Fe_3O_4@TiO_2$ MSs and 0.37 g of NH_4F were dispersed in a mixture of 66 mL of ethanol and 34 mL H_2O under mechanical stirring for 60 min. The mixture was hydrothermally treated at 180 °C in a Teflon-lined stainless steel autoclave (200 mL in capacity) for 24 h. The as-prepared products were washed with ultrapure water for 3 times to remove any ionic impurities, and dried at 80 °C overnight.

2.4. Synthesis of $Fe_3O_4@TiO_2@Au$ MSs

The as-prepared $Fe_3O_4@TiO_2$ MSs were dissolved in 200 mL of ethanol and 0.15 mL of APTMS, then the mixture was refluxed at 85 °C for 4 h. The products were washed with ethanol for 3 times and redispersed in 100 mL of ethanol for further use. Thus the APTMS modified $Fe_3O_4@TiO_2$ MSs were obtained. Citrate-stabilized Au NPs with an average diameter of ~10 nm were prepared according to the methods reported.[32,33] The pH of the Au NPs and modified $Fe_3O_4@TiO_2$ solution were adjusted to 5.0 by titration with 0.01 M HCl. Then 2.0 mL of modified $Fe_3O_4@TiO_2$ solution was added dropwise to 200 mL of the raw Au NPs solution and stirring for 15 min to obtain the proper density of Au NPs on the surface of the $Fe_3O_4@TiO_2$ MSs.

2.5. Characterization

The morphologies and sizes of the as-prepared samples were characterized by transmission electron microscopy (TEM) using a JEOL 2011 microscope (Japan) and scanning electron microscope (SEM) images using a JEOL JSM-6360LV microscope (Japan). The crystalline structure was investigated by X-ray power diffraction (RIGAKU, D/MAX 2550 VB/PC, Japan). The magnetic behavior was investigated using a vibrating sample magnetometer (VSM, Lake Shore 7304, Lake Shore, USA) with an applied field between -15 kOe and 15 kOe at room temperature. The UV-vis spectra were recorded on a UV-vis spectrometer (TU-1901, Beijing, China).

2.6. Catalytic reactions with $Fe_3O_4@TiO_2@Au$ MSs

The catalytic performance of the multifunctional $Fe_3O_4@TiO_2@Au$ MSs were investigated by the reduction of 4-NP to 4-AP in the presence of $NaBH_4$ as a model reaction. In a typical run, 5.85 mL of ultrapure water, 0.15 mL 5 mM of 4-NP solution, and 3.0 mL 20 mM of freshly prepared $NaBH_4$ aqueous solution were added into a 25 mL quartz beaker respectively, and the solution color turned to bright yellow rapidly. The pH of solution during the whole experimental process was controlled to 8.0 by titration with 0.01 M NaOH. Subsequently, 1.0 mL 5 wt% $Fe_3O_4@TiO_2@Au$ MSs was added to start the reaction. Agitation was provided by mechanical stirring. A UV lamp (365 nm, 70 W

cm^{-2}) or a high pressure Xenon lamp with a cutoff filter to block the UV light (>400 nm, 50 mW cm^{-2}) was used as the light source, which was placed 10 cm away from the reaction vessel. After irradiation, the sample was collected with a magnet and the
5 supernatant was extracted for the examination, and the intensity of absorption peak at 400 nm was monitored by UV-vis spectroscopy as a function of time. As the reaction was proceeding, the gradual change of the solution color from yellow to colorless can be observed. Figure 1 shows the schematic
10 diagrams for (a) the preparation of the multifunctional Fe$_3$O$_4$@TiO$_2$@Au MS and (b) the catalytic reduction of 4-NP with the multifunctional Fe$_3$O$_4$@TiO$_2$@Au MSs in the presence of NaBH$_4$ exposed to visible light.

15 **Figure 1.** Schematic diagrams for (a) the preparation of the multifunctional Fe$_3$O$_4$@TiO$_2$@Au MS and (b) the catalytic reduction of 4-NP with the multifunctional Fe$_3$O$_4$@TiO$_2$@Au MSs in the presence of NaBH$_4$ exposed to visible light.

3. Results and discussion

20 **3.1. Characterization of the triplex Fe$_3$O$_4$@TiO$_2$@Au core-shell MSs**

The triplex Fe$_3$O$_4$@TiO$_2$@Au core-shell MS was composed of a Fe$_3$O$_4$ magnetic core, a TiO$_2$ interlayer, and a layer of Au NPs shell outside. The well-defined Fe$_3$O$_4$ MSs with a narrow size
25 distribution and a mean diameter of ~400 nm were first synthesized through a robust solvothermal reaction (Figure 2a), the magnetic core ensure the easy separate of the catalysts from the reaction mixture. Close observation revealed that the uniform gray interlayer of TiO$_2$ with a thickness of about 35 nm provide a
30 continuous coverage of the magnetic Fe$_3$O$_4$ MS (Figure 2b), which not only are beneficial to the absorption of reactants but also ensure the degradation of organic products so that the MSs can be reused. Then, the resultant Fe$_3$O$_4$@TiO$_2$ core-shell MSs are modified with APTMS to render the particle surfaces with
35 amino groups. Finally, to mix the modified core-shell Fe$_3$O$_4$@TiO$_2$ MSs with citrate-stabilized Au NPs leading to the graft of Au NPs onto the surfaces of Fe$_3$O$_4$@TiO$_2$ MSs (Figure 2c, 2d). The Au NPs with a mean diameter of 10 nm were well-dispersed on the surface of Fe$_3$O$_4$@TiO$_2$ core-shell MS, and no
40 aggregation was observed.

Figure 3 shows X-ray diffraction (XRD) patterns of (blue) Fe$_3$O$_4$ MSs, (red) Fe$_3$O$_4$@TiO$_2$ MSs and (black) Fe$_3$O$_4$@TiO$_2$@Au MSs during different stages. The characteristic broad diffraction peaks shown in wide-angle XRD patterns can
45 be indexed to the spinel Fe$_3$O$_4$, anatase TiO$_2$ and cubic phase Au

NPs in the composite MSs. The specific XRD of Fe$_3$O$_4$ is characterized by six peaks positioned at 2θ values of 30.0°, 35.3°, 42.9°, 53.5°, 57.0° and 62.4°, corresponding to the [220], [311], [400], [422], [511] and [440] lattice planes of the cubic phase of
50 Fe$_3$O$_4$ (JCPDS card No. 01-075-0449), respectively. As shown in Figure 3 (red), after the coating of a ~35 nm TiO$_2$ layer and subsequent hydrothermal treatment, by comparison with the patterns of Fe$_3$O$_4$, that of the Fe$_3$O$_4$@TiO$_2$ show several additional peaks, which can be attributed to the anatase phase of
55 TiO$_2$. The reflections from the [101], [004], [200] and [105] planes of the anatase phase (JCPDS card No.01-075-2545) contribute the extra peaks located at 25.3°, 37.9°, 48.0° and 53.9°. It can be clearly shown in Figure 3 (black) that after loading 10 nm Au NPs on the surface of the Fe$_3$O$_4$@TiO$_2$ MS, the additional
60 diffraction peaks can be indexed to the cubic phase of Au (JCPDS card No.00-004-0784). The characteristic XRD patterns of Fe$_3$O$_4$@TiO$_2$@Au MSs imply that the current system is suitable for the synthesis.
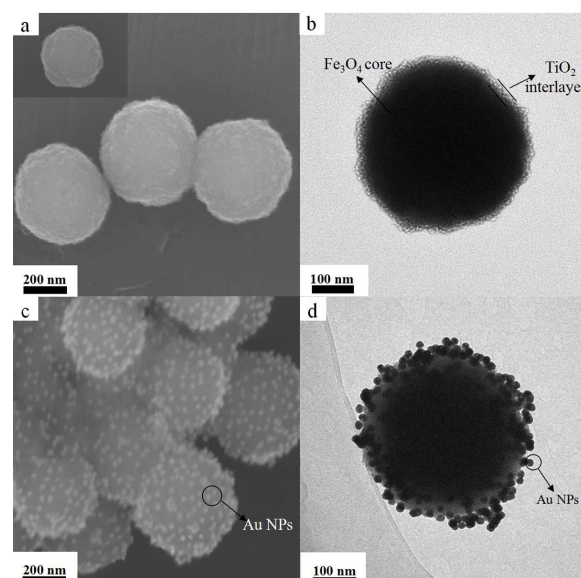
65 **Figure 2** (a) SEM image of Fe$_3$O$_4$ MS. (b) TEM image of Fe$_3$O$_4$@TiO$_2$ core-shell MSs with a uniform TiO$_2$ shell thickness of 35 nm. (c) SEM image of Fe$_3$O$_4$@TiO$_2$@Au (10 nm) and (d) the corresponding magnified TEM image.
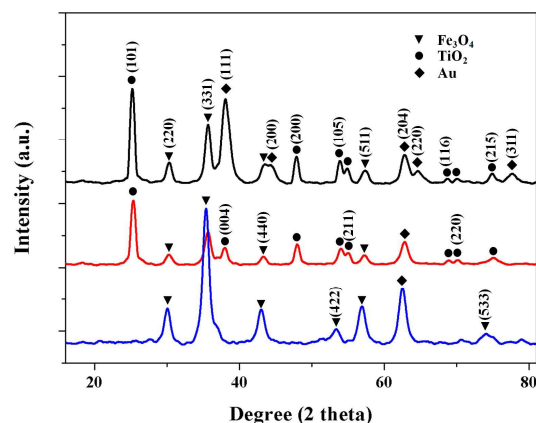
70 **Figure 3.** XRD patterns of (blue) Fe$_3$O$_4$, (red) Fe$_3$O$_4$@TiO$_2$ and (black) Fe$_3$O$_4$@TiO$_2$@Au MSs.

Figure 4 shows the magnetic hysteresis loops of the bare Fe_3O_4, $Fe_3O_4@TiO_2$, and $Fe_3O_4@TiO_2@Au$ MSs at room temperature. As shown, they exhibited superparamagnetic behavior and little hysteresis, remanence and coercivity due to the fact that the

5 particles were composed of ultrafine magnetite nanocrystals. The magnetic saturation (Ms) value of Fe_3O_4 MSs is about 53.2 emu/g, and that of $Fe_3O_4@TiO_2$ and $Fe_3O_4@TiO_2@Au$ are 41.1 and 22.2 emu/g, respectively. By comparison, decrease in magnetization is mainly attributed to the decrease in the density of Fe_3O_4 in the

10 obtained composites after coating with TiO_2 and then Au. However, it should be noted that the $Fe_3O_4@TiO_2@Au$ still showed strong magnetization, which suggested their suitability for magnetic separation. With the use of external magnetic field, the materials were quickly attracted to one side of the vial with

15 several seconds and the solution become transparent, as illustrated in the physical photograph (Figure 4 inset).
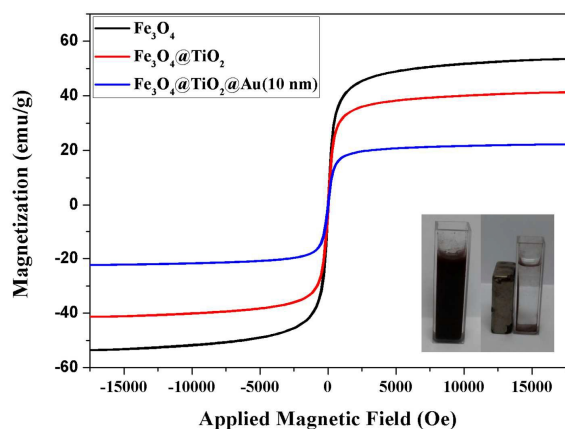
Figure 4. Magnetization curves of the Fe_3O_4, $Fe_3O_4@TiO_2$ and $Fe_3O_4@TiO_2@Au$ MSs, respectively. The inset pattern is a photograph of the
20 magnetic separation.

3.2. Application of the $Fe_3O_4@TiO_2@Au$ MSs for the catalytic reduction of 4-NP

4-NP is one of the most common organic pollutants in industrial and agricultural wastewater that is difficult to degrade,[16] while 4-
25 AP is a kind of useful raw material in medicine and the chemical industry. To investigate the catalytic activity of $Fe_3O_4@TiO_2@Au$ MSs, the catalytic reduction of 4-NP to their corresponding daughter derivatives 4-AP in the presence of $NaBH_4$ was chosen as the model reaction. The reduction reaction
30 is easy to follow for the reason that only one kind of product (4-AP) is obtained and the system can be monitored by UV-vis absorbance at 400 nm. This process can be monitored by the UV-vis spectrum for the reason that 4-NP and 4-AP have different absorption wavelengths (400 nm and 300 nm, respectively) in the
35 UV-vis range.[34] Figure 5 shows the pure 4-NP solution exhibited a distinct spectral profile with an maximal absorbance at 317 nm, the absorbance peaks shift to 400 nm was observed immediately as soon as the $NaBH_4$ solution was added, which correspond to a color change from light yellow to bright yellow for the formation
40 of 4-nitro-phenolate ion in alkaline condition,[35,36] as illustrated in the physical photograph (Figure 5 inset). And there is no change in the absorbance at 400 nm over time, as shown in Figure 6, which confirmed that the reaction cannot be pushed forward with $NaBH_4$ solution only.
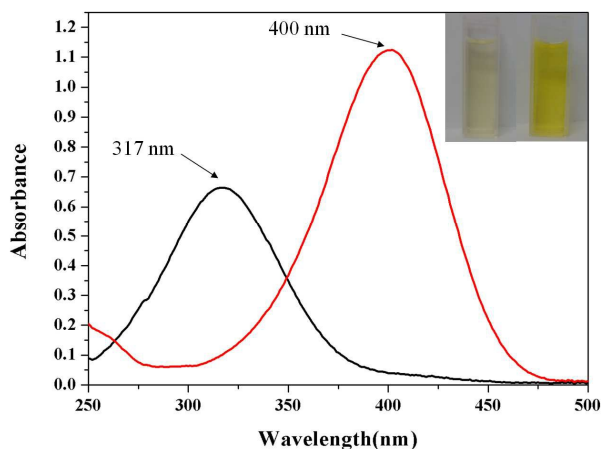
45 **Figure 5.** UV-vis absorption spectra of 4-NP (red line) with and (black line) without $NaBH_4$ solution.
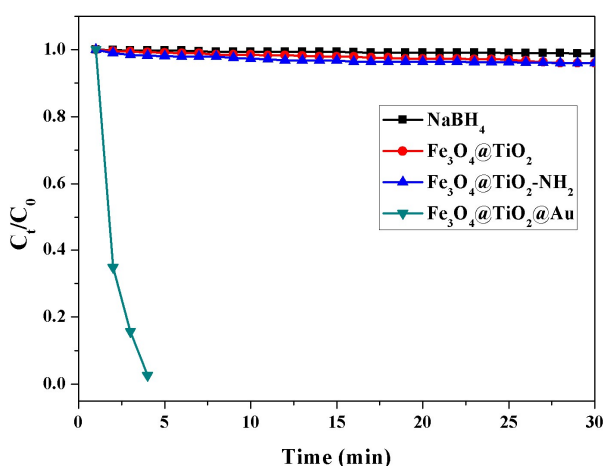
Figure 6. C_t/C_0 versus reaction time for the reduction of 4-NP with
50 $NaBH_4$ (black line), $Fe_3O_4@TiO_2$ MSs (red line), $Fe_3O_4@TiO_2$-NH_2 MNPs (blue line) and $Fe_3O_4@TiO_2@Au$ MSs (green line), respectively.

When evaluating the catalytic activity of $Fe_3O_4@TiO_2@Au$ MSs, that of $Fe_3O_4@TiO_2$ and APTMS modified $Fe_3O_4@TiO_2$ was investigated in advance. As shown in Figure 6, there is no
55 change in the UV-vis absorbance at 400 nm meaning that neither $Fe_3O_4@TiO_2$ nor APTMS modified $Fe_3O_4@TiO_2$ has catalytic activity to the reduction of 4-NP. The time-dependent UV-vis spectra of the reaction running in the presence of $Fe_3O_4@TiO_2@Au$ MS as catalysts as well as being exposed to
60 light was unambiguously exhibited in Figure 7 a. The absorption intensity of 4-NP at 400 nm significantly decrease the elapsed time when the catalysts were introduced accompanied with the appearance of absorption peak at 300 nm. As the reaction went on, the absorption intensity at 400 nm decreased along with the
65 increase of that at 300 nm. The full reduction of 4-NP was completed within 3 min by the observation of a fading and ultimate bleaching of the bright yellow colour of the reaction mixture. The syneristic effect of each component could be explored by the contrast of catalytic reduction run with
70 $Fe_3O_4@TiO_2@Au$ MS, $TiO_2@Au$ composite spheres, Fe_3O_4 MS and Au NPs subjected to different conditions including the exposure to visible light or not as shown in Figure 7. As shown in Figure 7 b, the full reduction could be completed within 6
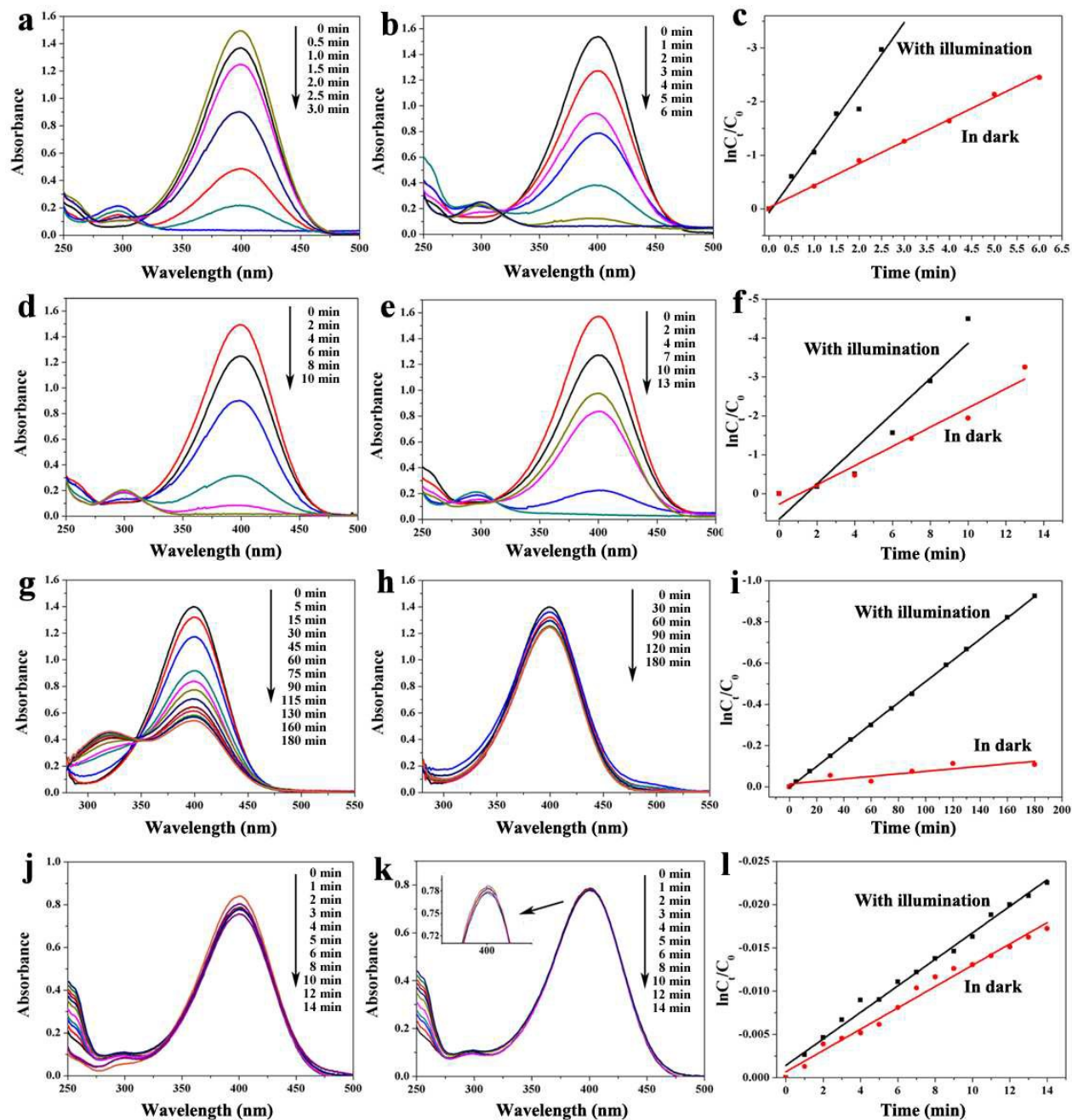
Figure 7. Catalytic reduction of 4-NP conducted in different conditions: $Fe_3O_4@TiO_2@Au$ MS with illumination (a), in dark (b); $TiO_2@Au$ with illumination (d), in dark (e); Fe_3O_4 MS with illumination (g), in dark (h); Au NPs with illumination (j), in dark (k), $\ln(C_t/C_0)$ versus the reaction time for the reduction of 4-NP over $Fe_3O_4@TiO_2@Au$ MS (c), $TiO_2@Au$ (f), Fe_3O_4 MS (i) and Au NPs (l) with illumination (black) and in dark (red) at 25 °C. C_0 and C_t is the absorption peak at 400 nm initially and at time t.

minutes in dark. When the system is in dark, the effect of photocatalysis was suppressed and noble metal catalysis play a dominant role. When the system was exposed to visible light but accompanied by the addition of $TiO_2@Au$ composites spheres as catalyst, as shown in Figure 7 d, the reaction is completed within 10 min with full reduction of 4-NP, and by comparison, the full reduction was completed within 13 min in dark (Figure 7 e). When the system was performed with Fe_3O_4 MS as catalysts, small reduction of 4-NP was observed exposed to visible light

(Figure 7 g) and no obvious reduction of 4-NP was noticed (Figure 7 h) even more than 180 min. When Au NPs (10 nm) alone served as catalysts, 4-NP has hardly any reduction with illumination or not (Figure 7 j, k). As the initial concentration of $NaBH_4$ is far higher than reactants, it is considered to remain constant throughout the whole reaction process. So the reaction is assumed to be independent of the concentration of $NaBH_4$, and a pseudo first-order kinetic equation could be applied to evaluate the catalytic rate.[37-39] In addition, most of the photocatalytic

reactions follow the Langmuir-Hinshelwood adsorption model,[40] and the L-H model can also be simplified to a pseudo-first-order expression. The absorption intensity of 4-NP is proportional to the concentration in the medium. Hence, the kinetic equation for the reduction could be written as follows:

$$\frac{dC_t}{dt} = \frac{dA_t}{dt} = kC_t = kA_t \text{ or } \ln\left(\frac{C_t}{C_0}\right) = \ln\left(\frac{A_t}{A_0}\right) = -kt$$

C_t is the concentration of 4-NP at time t and k is the apparent rate constant. Linear relationships between $\ln(C_t/C_0)$ and the reaction time are displayed in Fig 7 c, f, i, l, which matched well with the first-order reaction kinetics. The rate constant k (Figure 7 c_{black}) was calculated to be 1.180 min^{-1} at 25 °C exposed to visible light, which was higher than that reported for the same catalytic conversion using catalysts based on Au or Ag nanoparticles with varying morphologies and sizes.[41,42,14] And the values of k are 0.421 min^{-1} (Figure 7 c_{red}) in dark, 0.452 min^{-1} with illumination and 0.247 min^{-1} in dark (Figure 7 f), 0.00515 min^{-1} with illumination and 6.08E^{-4} min^{-1} in dark (Figure 7 i), 0.00153min^{-1} with illumination and 0,00123 min^{-1} in dark (Figure 7 l) respectively.

Figure 8 depicts the performance of the Fe$_3$O$_4$@TiO$_2$@Au MSs as catalysts in the reduction of 4-NP to 4-AP by NaBH$_4$ exposed to visible light. One of prominent features of noble metal is the LSPR. The LSPR refers to the oscillation of the metal's free electrons in phase with the varying electric field of the incident light.[43,44] When the system is irradiated by visible light, the electron density decreases on one side of the particle and increases on the other, facilitating the adsorption of BH$_4^-$ onto Au NPs. The reduction action occurred via electrons transfer from the donor BH$_4^-$ to the acceptor 4-NP after both adsorbed onto the particles surface. The hydrogen atom from the hydride, attacked 4-NP molecules to reduce it to 4-AP after the electron transfer to Au NPs.[45] The photocatalysis occurred simultaneously accompanied with the generation of degradation products.
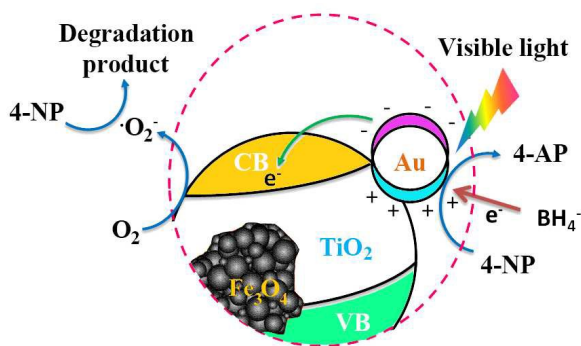
Figure 8. Schematic and photographic representation of the performance of Fe$_3$O$_4$@TiO$_2$@Au MSs as catalysts in the reduction of 4-NP by NaBH$_4$ exposed to visible light.

In general, heterogeneous catalysis proceed following the five independent steps:[46,47] (1) transfer of the reactant to the reaction surface, (2) absorption of reactant onto the active sites, (3) redox reactions, (4) desorption of the products and (5) transfer of products away from the surface. Any process beneficial to the five steps above may contribute to the catalytic performance enhancement. The uses of noble metal nanoparticles (Au NPs) benefit the catalytic reaction from not only the catalytic effects of

noble metal itself but also the distinct feature LSPR. This will bring some benefits to the catalysis. LSPR can heat up the local environment leading to the increase of the mass transfer of the reactants or products and then the enhancement of the reaction rates. The heating effects come from the collision electrons with the ionic lattice of the metal nanoparticles within 0.7 ps,[48] and the phonon-phonon relaxation coupled with the metal lattice and the semiconductor lattice.[49] Typically, the heating effects work efficiently in small nanoparticles (below 30 nm).[50-52] When the noble nanoparticles were in the state of LSPR, the absorption of reactant molecules onto the surface will be enhanced by dipole-dipole interactions. Since the local electric filed caused by LSPR is a fast-varying dipole and 4-NP are polar, 4-NP may be attracted to a metal surface by such dipole-dipole reaction. Metal nanoparticles can also provide a fast lane for charge transfer and the surface can be served as a charge-trap center to host more active sites for the interaction with molecules absorbed on it.[53] In the view of the five steps, the LSPR, the charge trapping and fast transfer and the large of contact areas contribute to the reaction rate, thus benefiting the step 3;[47,54] the heating effects can not only enhance the reaction rate but also accelerate the solution mixing and benefits step 1, 3, 4 and 5;[55] the enhancement of reactant absorption can benefit step 2. These contributions lead to the enhancement of the catalytic rates. In addition, the effects of semiconductor part cannot be ignored. TiO$_2$ is one kind of high-performance photocatalytic materials but confined to the large bandgaps and only absorb the light in the near ultraviolet (UV) region (wavelength <400 nm). The loading of Au NPs onto TiO$_2$ can make it response to the visible-light and perform its photocatalytic activity. The synergy of noble metal-catalysis and photocatalysis contribute to the high rate constant of the reduction of 4-NP (Figure 7 a, d, c_{black}, f_{black}). When the reaction system is in dark, no photocatalysis from semiconductor performed, leaving only the noble-metal catalysis. (Figure 7 b, e, c_{red}, f_{red}). To verify the synergy of each components, the experiment catalyzed by TiO$_2$@Au, Fe$_3$O$_4$ MS and Au NPs (10 nm) was performed. And the results were shown in Figure 7 d, e, f, h, i, j, k, l. The catalytic activity of Au NPs is strongly dependent on the size, and only catalysts with Au particles below 5 nm show catalytic activity.[1] In the article, the size of Au NPs loaded on the spot is around 10 nm. So, as Au NPs synthesized serve as catalysts alone for the reduction of 4-NP, it showed little catalytic activity. (as shown in Figure 7 j, k), meanwhile the aggregation of Au NPs without any support may also lead to reduction of activity. When the Au NPs are loaded onto TiO$_2$ for the formation of TiO$_2$@Au. The composites exhibit catalytic activity. It can be explained as follows: (1) the synergy of two components, (2) the loading of Au NPs on TiO$_2$ not only avoid the aggregation of Au NPs but also provide more active sites. The mesoporous structure of TiO$_2$ is beneficial for the adsorption of reactant molecules, that is to say, it can increase the contact chances for reactants and catalysts which is better than the random collision for Au NPs alone. The reduction proceeded under the condition of light-on better than that of light-off can be attributed to the assistance of visible light which contribute to the photocatalytic effect of TiO$_2$. (as shown in Figure 7 d, e, f) The catalytic activity of Fe$_3$O$_4$ is very low and the location of it inside also limited the contact with reactants, the activity cannot be

compared with other catalysts. (Figure 7 g, h, i). Fe_3O_4 NPs can absorb visible light. The Fe_3O_4 core of the composites not only exhibits the magnetic property for the easy separation of catalysts from the reaction solution but also enhance the adsorption of
5 visible light which can promote the catalytic process. (Figure 7 a, d).

3.3. Recovery ability of the $Fe_3O_4@TiO_2@Au$ MS

One of the main advantages of as-prepared $Fe_3O_4@TiO_2@Au$ MSs is the potential recyclability. By the external magnetic field,
10 it is convenient for $Fe_3O_4@TiO_2@Au$ MSs to separate from the reaction medium within several minutes. In addition, if the obtained $Fe_3O_4@TiO_2@Au$ MSs can self-clean the molecules absorbed on it, the reuse ability can be realized.[56] The self-cleaning activity was evaluated by monitoring the residue
15 characteristic absorption band at 300 nm to measure the degradation rate of 4-AP under a UV lamp (365 nm, 70 W cm^{-2}) or a high pressure Xenon lamp with a cutoff filter to block the UV light (< 400 nm, 50 W cm^{-2}). It has been shown recently that metal NPs, such as Au and Ag, embedded in the matrix of TiO_2
20 can enhance the photocatalytic activity of TiO_2 under visible light irradiation.[57-59] Figure 9 a show the concentration change of the aqueous 4-AP solution versus irradiation time. As can be seen, the $Fe_3O_4@TiO_2@Au$ MS exhibits the excellent photocatalytic performance. Most of the photocatalytic reactions follow the
25 Langmuir-Hinshelwood adsorption model,[46] and the L-H model can be simplified to a pseudo-first-order expression: $\ln(C_0/C) = kt$ (where C_0 and C are the initial concentration and the concentration of 4-AP at the exposure time, t, respectively, and k is the linear plots of $\ln(C_0/C)$ versus irradiation time t is attained)
30 and the photocatalytic reaction rate of $Fe_3O_4@TiO_2@Au$ is 0.096 min^{-1} as shown in Figure 9 b. Thus, the $Fe_3O_4@TiO_2@Au$ MS can achieve the self-cleaning property under visible light irradiation. And then the MS was washed with deionized water and collected by magnet. Then the MS were dried for the
35 catalytic reduction again. As shown in Figure 9 c, MS can be recycled and reused for at least 8 times with a stable conversion of ~92%. The decrease of conversion after 8 cycles may be attributed to the loss of catalysts with the repeated magnetic separation.

40 ## 4. Conclusions

In conclusion, we have successfully synthesized the novel multifunctional $Fe_3O_4@TiO_2@Au$ core-shell composites. The $Fe_3O_4@TiO_2@Au$ MSs exhibited excellent catalytic activity for the reduction of 4-NP in the presence of $NaBH_4$ under visible
45 light with convenient magnetic separability and fine recoverability. The synergy of noble metal-catalysis and photocatalysis contribute to the high rate constant of the reduction of 4-NP (k = 1.180 min^{-1} at 25 °C). Especially the $Fe_3O_4@TiO_2@Au$ MSs can be recycled and reused for at least 8
50 times with a stable conversion of ~92%. This approach provides a useful platform based on the synergy of varying components under suitable conditions to optimize the catalytic ability. Additionally, these core-shell magnetic microspheres can be extended to various advanced applications such as environmental
55 protection, chemical biosensors, nanoelectronics and so on.
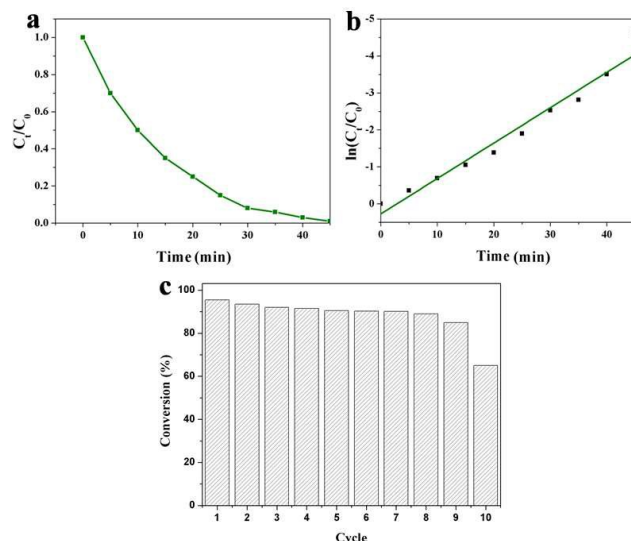
Figure 9. Photocatalytic degradation study of 4-AP on $Fe_3O_4@TiO_2@Au$ MS (a) and $\ln(C_0/C)$ versus time line study on $Fe_3O_4@TiO_2@Au$ under visible light irradiation (b). The recovery ability of $Fe_3O_4@TiO_2@Au$ MS as a
60 catalyst for the reduction of 4-NP with the presence of $NaBH_4$ (c).

Notes and references

*Key Laboratory for Ultrafine Materials of Ministry of Education, School of Materials Science and Engineering, East China University of Science
70 and Technology, Shanghai 200237, China. E-mail: yhzhu@ecust.edu.cn; czli@ecust.edu.cn*

1　B. Hvolbæk, T. V.W. Janssens, B. S. Clausen, H. Falsig, C. H. Christensen, J. K. Nørskov, *Nanotoday*, 2007, **2**, 14.
2　Haruta, M., et al., *Chem. Lett.*, 1987, **16**, 405.
75 3　M. Haruta, N. Yamada, T. Kobayashi and S. Lijima, *J. Catal.*, 1989, **115**, 301.
4　A. Orlov, D. A. Jefferson, N. Macleod and R. M. Lambert, *Catal. Lett.*, 2004, **92**, 41.
5　S. Praharaj, S. Nath, S. K. Ghosh, S. Kundu and T. Pal, *Langmuir*,
80 2004, **20**, 9889.
6　J. Zeng, Q. Zhang, J. Chen and Y. Xia, *Nano Lett.*, 2010, **10**, 30.
7　J. Gong and C. B. Mullins, *Acc. Chem. Res.*, 2009, **42**,1063.
8　E. Gross, X. Z. Shu, S. Alayoglu, H. A. Bechtel, M. C. Martin, F. D. Toste and G. A. Somorjai, *J. Am. Chem. Soc.,* 2014, **136**, 3624.
85 9　J. Li, C.Liu and Y. Liu, *J. Mater. Chem.*, 2012, **22**, 8426.
10　K. Kuroda, T. Ishida and M. Haruta, *J. Mol. Catal. A: Chem.*, 2009, **298**, 7.
11　J. Zheng, Y. Dong, W. Wang, Y. Ma, J. Hu, X. Chen and X. Chen, *Nanoscale*, 2013, **5**, 4894.
90 12　F. Lin and R. Doong, *J. Phys. Chem. C*, 2011, **115**, 6591.
13　A. A. Ismail, A. Hakki and D. W. Bahnemann, *J. Mater. Catal.A*, 2012, **358**, 145.
14　Y. Zhang, S. Liu, W. Lu, L. Wang, J. Tian and X. Sun, *Catal. Sci. Technol*, 2011, **1**, 1142.
95 15　L. Han, C. Zhu, P. Hu and S. Dong, *RSC Adv*., 2013, **3**, 12568.
16　Y. C. Chang and D. H. Chen, *J. Hazard. Mater.*, 2009, **165**, 664.
17　Y. Zhu, J. Shen, K. Zhou, C. Chen, X. Yang and C. Li, *J. Phys. Chem. C*, 2011, **115**, 1614.
18　K. Esumi, R. Isono and T. Yoshimura, *Langmuir*, 2004, **20**, 237.

19 Y. Zhang, S. Liu, W. Lu, L. Wang, J. Tian and X. Sun, *Catal. Sci. Technol.*, 2011, **1**, 1142.

20 G. Chang, Y. Luo, W. Lu, X. Qin, A. M. Asiri, A. O. Al-Youbibc and X. Sun, *Catal. Sci. Technol.*, 2012, **2**, 800.

21 J. Zheng, Y. Dong, W. Wang, Y. Ma, J. Hu, X. Chen and X. Chen, *Nanoscale*, 2013, **5**, 4894.

22 S. Linic, P. Christopher and D. B. Ingram, *Natrue Mater.*, 2011, **10**, 911.

23 E. Marais and T. Nyokong, *J. Hazard. Mater.*, 2008, **152**, 293.

24 W. Sun, J. Li, G. Yao, M. Jiang and F. Zhang, *Catal. Commun.*, 2011, **16**, 90.

25 T. L. Lai, K. F. Yong, J. W. Yu, J. H. Chen, YY Shu and C. B. Wang, *J. Hazard. Mater.*, 2011, **185**, 366.

26 M. Panizza and G. Cerisola, *Water Res.*, 2009, **43**, 339.

27 Y. Zhang, L. Wu, W. Lei, X. Xia, M. Xia and Q. Hao, *Electrochim. Acta*, 2014, **146**, 568.

28 Y. Du, H. Chen, R. Chen and N. Xu, *Appl. Catal. A*, 2004, **277**, 259.

29 S. Saha, A. Pal, S. Kundu, S. Basu and T. Pal, *Langmuir*, 2010, **26**, 2885.

30 J. Liu, Z. K. Sun, Y. H. Deng, Y. Zou, C. Y. Li, X. H. Guo, L. Q. Xiong, Y. Gao, Y. F. Li and D. Y. Zhao, *Angew. Chem. Int. Ed.*, 2009, **48**, 5875.

31 W. Li, J. P. Yang, Z. X. Wu, J. X. Wang, B. Li, S. S. Feng, Y. H. Deng, F. Zhang and D. Y. Zhao, *J. Am. Chem. Soc.*, 2012, **134**, 11864.

32 J. Kimling, M. Maier, B. Okenve, V. Kotaidis, H. Ballot and P. Plech, *J. Phys. Chem. B*, 2006, **110**, 15700.

33 C. Ziegler and A. Eychmuller, *J. Phys. Chem. B*, 2011, **115**, 4502

34 Y. Qiu, Z. Ma and P. Hu, *J. Mater. Chem. A*, 2014, **2**, 13471.

35 K. Hayakawa, T. Yoshimura and K. Esumi, *Langmuir*, 2003, **19**, 5517.

36 S. Praharaj, S. Nath, S. K. Ghosh, S. Kundu and T. Pal, *Langmuir*, 2004, **20**, 9889.

37 J. Ge, Q. Zhang, T. Zhang and Y. Yin, *Angew. Chem.*, 2008, **120**, 9056.

38 J. M. Herrmann, *Catal. Today*, 1999, **53**, 115.

39 K. S. Shin, Y. K. Cho, J.-Y. Choi and K. Kim, *Appl. Catal. A*, 2012, **413**, 170.

40 S. J. Zhuo, M. W. Shao and S. T. Lee, *ACS Nano*, 2012, **6**, 1059.

41 D. M. Dotzauer, S. Bhattacharjee, Y. Wen and M. L. Bruening, *Langmuir*, 2009, **25**,1865.

42 Y. Mei, Y. Lu, F. Polzer and M. Ballauff, *Chem. Mater.*, 2007, **19**, 1062.

43 B. Naik, S. Hazra, V. S. Prasad and N. N. Ghosh, *Catal.Commun.*, 2011, **12**, 1104.

44 X. Du, J. He, J. Zhu, L. Sun and S. An, *Appl. Surf. Sci.*, 2012, **258**, 2717.

45 J. M. Herrmann, *Top. Catal.*, 2006, **39**, 3.

46 J. M. Herrmann, *Top. Catal.*, 2005, **34**, 49.

47 X. Zhang, Y. L. Chen, R.-S. Liu and D. P. Tsai, *Rep. Prog. Phys.*, 2013, 76, 1.

48 C. K. Sun, F. Vallée, L. H. Acioli, E. P. Ippen and J. G. Fujimoto, *Phys. Rev. B*, 1994, **50**, 15337.

49 S. Link and M. A. El-Sayed, *Ann. Rev. Phys.Chem.*, 2003, **54**, 331.

50 P. Christopher, D. B. Ingram and S. Linic, *J. Phys. Chem. C*, 2010, **114**, 9173.

51 J. R. Adleman, D. A. Boyd, D. G. David and D. Psaltis, *Nano Lett.*, 2009, **9**, 4417.

52 C. W. Yen and M. A. El-Sayed, *J. Phys. Chem. C*, 2009, **113**, 19585.

53 J. R. Lombardi and R. L. Birke, *J. Phys. Chem. C*, 2008, **112**, 5605.

54 K. Awazu, M. Fujimaki, C. Rockstuhl, J. Tominaga, H. Murakami, Y. Ohki, N. Yoshida and T. Watanabe, *J. Am. Chem. Soc.*, 2008, **130**, 1676.

55 S. Sun, W. Wang, L. Zhang, M. Shang and L. Wang, *Catal. Commun.*, 2009, **11**, 290.

56 X. Zhang, Y. Zhu, X. Yang, Y. Zhou, Y. Yao and C. Li, *Nanoscale*, 2014, **6**, 5971.

57 X. D. Wang, T. Dornon, M. Blackford and R. A. Caruso, *J. Mater.Chem.*, 2012, **22**, 11701.

58 O. Akhavan and E. Ghaderi, *Surf. Coat. Technol.*, 2010, **204**, 3676.

59 X. D. Wang and R. A. Caruso, *J. Mater, Chem.*, 2011, **21**, 20.